Translational Oncology 14 (2021) 101175

Contents lists available at ScienceDirect

Translational Oncology

journal homepage: www.elsevier.com/locate/tranon

Original research

The significance of SMARCB1 in the pathogenesis of renal cell carcinoma with rhabdoid features

Yi-Wen Wang [a], Hsiang-Lin Song [b], Cheng-Yao Chiang [a], Hong-Fang Song [c], Hong-Yi Chang [d], Chien-An Chu [a], Yih-Lin Tuan [c], Kun-Hao Tsai [c], Yin-Chien Ou [e], Nan-Haw Chow [a,b,c,**], Yuh-Shyan Tsai [e,*]

[a] Departments of Pathology, College of Medicine, National Cheng Kung University, Tainan, TAIWAN
[b] Department of Pathology, National Cheng Kung University Hospital, Tainan, TAIWAN
[c] Institute of Molecular Medicine, College of Medicine, National Cheng Kung University, Tainan, TAIWAN
[d] Department of Biotechnology and Food Technology, College of Engineering, Southern Taiwan University of Science and Technology, Tainan, TAIWAN
[e] Departments of Urology, College of Medicine, National Cheng Kung University, Tainan, TAIWAN

ARTICLE INFO

Keywords:
Renal cell carcinoma
Rhabdoid differentiation
SMARCB1
Epidermal growth factor receptor
Erlotinib

ABSTRACT

Background: Renal cell carcinoma with rhabdoid features (RCC-RF) is an aggressive histologic variant in the adults and is usually unresponsive to standard chemotherapy.
Methods: Expression of *SMARCB1/INI1* was examined in primary RCC-RF (n = 5). Stable *INI1* with/without prostaglandin E2 receptor 1 (*EP1*) knockdown cell lines were created in the ACHN and 786-O RCC cell lines and measured for epidermal growth factor receptor (EGFR)-related signaling pathways. Chemosensitivity to targeted drugs *in vitro* was tested after knocking down of *INI1* in both cell lines. The outcome of co-targeting of *INI1* and *EP1* in RCC was examined using a tumorigenicity assay.
Results: Expression of *INI1* was markedly reduced at both transcriptional and translational levels in primary RCC-RF. Immunohistochemical expression of INI1 protein was lost in the nuclei of rhabdoid cells compared with conventional RCC (n = 8). Using two cell lines with different genetic background, we showed that knocking down of *INI1* activates the EGFR signaling with up-regulated AKT and ERK pathways and sensitizes cancer cells to Erlotinib treatment *in vitro*. However, cell-line dependent effects were also demonstrated with reference to impact of *INI1* or *EP1* on cell growth, migration and response to Gefitinib or Everolimus treatment *in vitro*.
Conclusion: Inactivation of *INI1* may play a role in the pathogenesis of RCC-RF. Erlotinib is recommended in the management of patients with *INI1*-related RCC.

Background

Renal cell carcinoma (RCC) is the most common type of kidney cancer (85%) and accounts for 2–3% of all malignant neoplasms in adults [1]. Currently, 5-year survival ranges from 85% for patients with organ-confined disease after partial or radical nephrectomy to 10% in patients with metastatic disease [1]. For those with localized diseases, surgery and cryoablation are the preferred treatments. For metastatic disease, checkpoint inhibitor-based immunotherapy and targeted therapies, especially vascular endothelial growth factor (VEGF) targeting agents, are typically the main treatment options, and with removal of the kidney if eligible [1,2]. However, many tumor subtypes, papillary

Abbreviations: ARRIVE, Animal Research Reporting In Vivo Experiments; ELISA, Enzyme Linked Immunosorbent Assay; EMA, Epithelial Membrane Antigen; EP1, Prostaglandin E2 Receptor 1; IHC, Immunohistochemistry; INI1, Integrase Interactor 1; KD, Knockdown; MRT, Malignant Rhabdoid Tumor; MTT, 3-(4,5-Dimethylthiazol-2-yl)-2,5-diphenyltetrazolium bromide; NOD/SCID, Nonobese Diabetic/Severe Combined Immunodeficiency; NSE, Neuron-specific Enolase; PCR, Polymerase Chain Reaction; PDGFR, Platelet-derived Growth Factor Receptors; PGE2, Prostaglandin E2; RCC, Renal Cell Carcinoma; RCC-RF, Renal Cell Carcinoma with Rhabdoid Features; RT-PCR, Reverse Transcription Polymerase Chain Reaction; SWI/SNF, Switch/Sucrose Non-Fermentable; VEGF, Vascular Endothelial Growth Factor.

* Corresponding author at: Department of Urology, College of Medicine, National Cheng Kung University, 1 University Road, Tainan City 70101, TAIWAN,
** Corresponding author at: Department of Pathology, College of Medicine, National Cheng Kung University, 1 University Road, Tainan City 70101, TAIWAN
E-mail addresses: chownh@mail.ncku.edu.tw (N.-H. Chow), youh@mail.ncku.edu.tw (Y.-S. Tsai).

https://doi.org/10.1016/j.tranon.2021.101175
Received 6 November 2020; Received in revised form 23 June 2021; Accepted 4 July 2021
Available online 6 July 2021

RCC (pRCC) for example, are resistant to targeted or immunotherapy [3]. Thus, a better understanding of molecular mechanisms underlying disease progression and drug resistance is indispensable to provide maximum therapeutic efficacy and improve patient prognosis.

Malignant rhabdoid tumor (MRT) is an aggressive tumor and predominantly occurs in the kidney and brain (atypical teratoid/rhabdoid tumors) of infants and young children. MRT has characteristic histological features of loosely cohesive polygonal cells with eccentric vesicular nuclei, prominent nucleoli, abundant eosinophilic inclusion-like cytoplasm, and immunoreactivity for both cytokeratin and vimentin [4]. Classical MRT has a mutation inactivation of integrase interactor 1 (*INI1/hSNF5*, SMARCB1, and BAF47) tumor suppressor gene at 22q23. The INI1 protein (47 kDa) is a core subunit of the switch/sucrose non-fermentable (hSWI/SNF) chromatin remodeling complex and is important in multiple nuclear processes, such as transcription, DNA replication, and DNA repair [5,6], and a negative regulator of cell cycle [7]. INI1 induces cell arrest at G0/G1 phase by directly repressing cyclin D1 and activating the cyclin-dependent kinase inhibitors $p16^{Ink4a}$ and $p21^{CIP}$. It can also control actin cytoskeleton network [8], which is implicated in tumor invasion and metastasis.

Foci of high-grade cancer cells with rhabdoid features may occur in around 4% of adult RCCs (RCC-RF) of several histological subtypes [9]. The rhabdoid cells have histological, immunohistochemical, and ultrastructural features reminiscent of MRTs with a characteristic epithelioid appearance, eccentric and enlarged nuclei, macronucleoli, and abundant cytoplasm [9–14, 15]. RCC-RF is usually related to advanced clinical staging and associated with a poor patient prognosis. Clinical observations reported that RCC-RF appears to respond to tyrosine kinase inhibitors (TKIs) of Sorafenib or Sunitinib [16–19]. Nevertheless, the molecular pathogenesis of RCC-RF remains ambiguous.

Both chromosome 3p loss and VHL gene mutation, the same genetic alterations of clear cell RCC (ccRCC), have been reported in RCC-RF [20]. A molecular genetic study also discovered combined loss of the *BAP1, PBRM1* and *TP53* suppressor genes in some of RCC-RFs [21]. Contradictory findings were reported in immunohistochemistry of rhabdoid cells [13,20,22–24]. For example, earlier studies showed retained nuclear INI1 expression in rhabdoid cells of several RCC variants: *e.g.*, cribriform, sarcomatoid and micropapillary [13]. In contrast, one study demonstrated loss of INI1 nuclear expression in all three cases of RCC-RF [23]. However, a recent large cohort study found variable losses of at least 1 SWI/SNF complex subunit in 21 of 32 cases (65%) of undifferentiated/rhabdoid component of RCC [24]. Notably, all 4 cases with a loss of *INI1* showed intact expression of the remaining SWI/SNF proteins, implying that *INI1* might be more oncogenic than other components of the complex.

This study was designed to investigate potential molecular mechanisms underlying *INI1* in the pathogenesis of RCC-RF. Current targeted therapy agents for RCC were tested on stable *INI1* knockdown (KD) cell lines *in vitro* to identify candidate drugs in the management of patients with RCC-RF.

Methods

Cell culture and chemicals

Two RCC cell lines (ACHN and 786-O) were selected for this model experiment. The ACHN cells harbor a pRCC specific mutation in *c-MET* without *VHL* mutations, while 786-O is a *VHL*-defective ccRCC cell line with HIF-1α overexpression [25]. Both cell lines were cultured in RPMI1640 (Gibco, Carlsbad, CA) with 10% fetal bovine serum (HyClone, Thermo Fisher Scientific, Boston, MA), 1% antibiotic- antimycotic solution (Caisson Lab, Inc., North Logan, UT). The *INI1* KD stable clones were selected by Blasticdin (Invitrogen Corp., Carlsbad, CA). The stable *INI1/* PGE2 receptor 1 (*EP1*) double KD pools were sorted by BD FACSAria™ cell sorter (Becton Dickinson, Miami, FL). Prostaglandin E2 (PGE2) was purchased from Cayman Chemical Company, Inc. (Ann Arbor, MI). MK-2894 was purchased from ApexBio Technology Inc. (Houston, TX). EGF was purchased from Invitrogen Corp. (Carlsbad, CA).

Microarray analysis

RNA (0.2 μg) of ACHN vector or *INI1* stable KD cell line was amplified by a Low Input Quick-Amp Labeling kit (Agilent Technologies, Santa Clara, CA) and labeled with Cy3 (CyDye, Agilent Technologies, Santa Clara, CA) during *in vitro* transcription process. The Cy3-labled cRNA (0.6 μg) was incubated with fragmentation buffer at 60 °C for 30 min, fragmented to an average size at about 50–100 nucleotides, and then pooled and hybridized to Agilent SurePrint G3 Human GE 8 × 60 K Microarray (Agilent Technologies, Santa Clara, CA) at 65 °C for 17 h. After washing and drying, microarrays were scanned with an Agilent microarray scanner (Agilent Technologies, Santa Clara, CA) at 535 nm for Cy3 and analyzed by Feature extraction10.5.1.1 software (Agilent Technologies, Santa Clara, CA). The normalization software was used to correct background intensity and quantify the signals for each feature.

Transient transfection

Cells were transfected with miRNA using Lipofectamine® LTX reagent (Invitrogen Corp., Carlsbad, CA). Cells were seeded 5×10^5 in 60 mm dishes or 6-well plate and allowed to achieve 50% to 70% confluence. The miRNA (3ug) was mixed with plus reagent in 100 ul serum free culture medium and Lipofectamine® LTX before use. The resulting mixture was incubated for 30 min at room temperature to form transfection complex. Then, transfection complex (~100 μl) was added dropwise to the well containing cells, mixed gently by rocking back and forth and incubated at 37 °C in a CO2 incubator for 48 h prior to testing for transgene expression. The specific miRNA sense sequences are as follows:

EP1:5′-TGCTGCGCAGTAGGATGTA-CACCCAAGTTTTGGCCACTGACTGACTTGGGTGTATCCTACTGCG-3′.

For stable ACNH1 INI1 KD and ACHN INI1&EP1 KD cell lines were selected in blasticidin after transient transfected with INI1 knockdown. The positive colonies were screening by INI1 Western blotting to confirm the INI1 knockdown efficiency.

RT-PCR (reverse transcription- polymerase chain reaction)

Total RNA was extracted by Trizol reagent (Invitrogen, Carlsbad, CA). The RNA (3 μg) was added in a sterile RNase-free micro-centrifuge tube and supplemented with 1 μg of Oligo(dT) to a total volume of 5 μl. The tubes were heated to 76 °C for 5 min to destroy secondary structure of RNA. Then, tubes were incubated on ice for 5 min. After spinning down, following components were added to the annealed primers/templates in the order of M-MLV RT 5X reaction buffer (5 μl), dNTP (10 mM, 1 μl), M-MLV RT (H–) (1 μl, 200 units), and nuclease-free water to a final volume of 20 μl.

Real-time (PCR) analysis

Total RNA was isolated using TRIzol according to manufacturer's instruction. Samples (2 μg) were reversely transcribed to synthesize first-strand cDNA using oligo dT and Moloney murine leukemia virus reverse transcriptase (Promega Corp., Madison, WI). A real-time PCR system (LightCycler™; Roche, Indianapolis, IN) and SYBR Green I labeling were used to measure the expression level of target genes.

Western blotting

Cells were lysed by radioimmunoprecipitation assay buffer (NaCl: 150 mM, NP-40:1%, sodium deoxycholate: 0.5%, Tris–HCl (pH 7.6): 50 rpm mM). The protease inhibitor mixture (1 mM NaVO4, 2 mM EGTA, 1

mM PMSF, 10 μg/mL aprotinin, 10 μg/mL leupeptin, 1 mM ethylene diamine tetra acetic acid) was added before use. Then, whole cell lysates were incubated on ice for 15 min and centrifuged at 14,000 rpm for 20 min. Total protein was measured by Bradford protein assay. According to size of target protein, a total of 30 μg - 50 μg proteins were separated by 6 - 10% sodium dodecyl sulfate polyacrylamide gel electrophoresis at 130 Vs for 15–20 min (for stacking gel), 160 Vs for 45–50 min (for running gel), and then transferred to 0.45 μm polyvinylidene fluoride membrane (Roche Applied Science) at 110 Vs for 80 min. The 5% skim milk or 5% bovine serum albumin was used for blocking at room temperature for 1 hr. Primary antibody was hybridized at 4 °C overnight, and then incubated with horseradish peroxidase-conjugated anti-mouse (1:10,000, Thermo Fisher Scientific, Boston, MA), anti-rabbit (1:2500, Thermo Fisher Scientific, Boston, MA) or anti-goat IgG antibody (1:2500, Santa Cruz, CA). The dilution of each antibody was as follows: epidermal growth factor receptor (EGFR) (1:1000, Santa Cruz, CA), phosphor-EGFR (Y1173) (1:1000, Abcam, Cambridge, MA), Akt (1:1000, GeneTex Inc., Irvine, CA), phosphor-Akt (ser473) (1:1000, Thermo Fisher Scientific, Boston, MA), phosphor-Erk1/2 (1:1000, Abcam, Cambridge, MA), Erk1/2 (1:1000, Abcam, Cambridge, MA), EP1 (1:500, Abcam, Cambridge, MA), EP4 (1:500, Abcam, Cambridge, MA), COX-1 (1:1000, GeneTex Inc., Irvine, CA), BAP-1 (D1W9B, 1:1000, Cell Signaling Technology Inc., Danvers, MA), PB1 (1:1000; GeneTex Inc., Irvine, CA), VEGF (1:1000, GeneTex Inc., Irvine, CA), VEGFC (1:1000, GeneTex Inc., Irvine, CA), and β-actin (1:5000, GeneTex Inc., Irvine, CA).

Cell viability assay

ACHN cells (1×10^3) and 786-O cells (2.5×10^2) were seeded per well in 96-well plate containing 100 μl medium and waited for attachment to the bottom. Anti-cancer drugs were treated with indicated doses of thymidylate synthase inhibitor (Capecitabine; Xeloda®) ranged from 0,1.25 μM 2.5 μM, 5 μM, 10 μM to 20 μM, anti-VEGF antibody (Bevacizumab; Avastin®) ranged from 0, 1.25 μM, 2.5 μM, 5 μM, 10 μM to 20 μM, mammalian target of rapamycin (mTOR) inhibitor (Everolimus) ranged from 0, 0.625 μM, 1.25 μM, 2.5 μM, 5 μM to 10 μM, VEGF receptor inhibitors of Sorafenib ranged from 0, 1.25 μM, 2.5 μM, 5 μM, 10 μM to 20 μM, and Sunitinib ranged from 0, 1.25 μM, 2.5 μM, 5 μM, 10 μM to 20 μM, and EGFR monotarget inhibitors of Gefitinib ranged from 0, 1.25 μM, 2.5 μM, 5 μM, 10 μM to 20 μM and Erlotinib ranged from 0.625 μM 0,1.25 μM 2.5 μM, 5 μM to 10 μM. They were dissolved in 10% serum medium and incubated for 72 hr. The supernatant was removed and replaced with 3-(4,5-Dimethylthiazol-2-yl)−2,5-diphenyltetrazolium bromide (MTT) solution (50 μl) (2 mg/ml, Invitrogen Corp., Carlsbad, CA.) in each well, incubated in 37 °C with 5% CO2 incubator for 4 h. The supernatant was removed and replaced with 50 μl dimethyl sulfoxide per well to dissolve purple formazan crystals. The absorbance (optical density) was measured at wavelength of 570 nm. All of target therapy drugs were got from Dr. Chia-Jui Yen (Department of Internal Medicine, College of Medicine, National Cheng Kung University).

Cell migration and invasion assays

The assay was performed in 24-well Transwell™ system which purchased from Corning® (Corning, NY). Briefly, transwell insert was put in 24-well plate. Then, cells (1.5×10^4 cell/well) were seeded in the transwell insert containing 200μl serum free medium in the upper chamber, and carefully added 600μl 10% serum medium to avoid air bubbles in the lower chamber. After incubation at 37 °C for 24 hrs., medium was removed and washed by PBS. The filter in the transwell insert was fixed by 100% methanol for 10 min. The non-migrated cells on the upper surface of membrane were removed by wiping with a cotton swab. The migrated cells to on the lower surface of membrane were stained with 2% crystal violet for 5 min. The number of migrated cells on the lower surface of membrane was examined under light microscope and analyzed by Image J software. Ten fields were counted per transwell filter in each group and each experiment was repeated in triplicate.

The invasion assay was performed using Corning® BioCoat™ Matrigel® Invasion Chambers (Corning, NY) with 8 mm pore size. The invasion chambers were put in 24-well plate. Then, cells (1×10^5) were seeded in invasion chambers containing 200μl serum free medium in the upper chamber and carefully added 600μl 10% serum medium to avoid air bubbles in the lower chamber. After incubation at 37 °C for 24 hrs., the matrigel in the invasion chambers was fixed by 100% methanol for 10 min. The non-invasive cells on the upper surface of membrane were removed by wiping with a cotton swab. The invasive cells to on the lower surface of membrane were stained with 2% crystal violet for 5 min. The number of invasion cells on the lower surface of membrane was examined under light microscope and analyzed by Image J software. Ten fields were counted per invasion chamber in each group and each experiment was repeated in triplicate.

Measurement of PGE2 by enzyme linked immunosorbent assay (ELISA)

To assay PGE2 production by ACHN stable cells, 5×10^5 cells were seeded into each well of a 6-well plate and cultured overnight. The medium was refreshed with serum-free RPMI-1640 at the following day and cultured for additional 24 hr. Cell-free media were prepared by centrifugation of supernatants to remove cell debris and stored at −80 °C before measurement. The PGE2 concentration was determined using a PGE2 ELISA kits (ENZO Life Sciences International, Inc., PA) according to the manufacturer's instructions.

Immunohistochemistry (IHC)

The IHC was performed according to standard procedure. Briefly, tissue sections were incubated at RT for 2 h with monoclonal antibody raised against INI1 (1:200, Santa Cruz Biotechnology, Inc., Santa Cruz, CA), VEGF (1:200, GeneTex Inc., Irvine, CA), VEGFC (1:200, GeneTex Inc., Irvine, CA), or EGFR (Santa Cruz Biotechnology, Inc., Santa Cruz, CA). The optimal dilution was determined by using human kidney as a positive control. Then, StrAviGen Super Sensitive MultiLink kit (BioGenex Laboratories, Inc., San Ramon, CA) was used to detect the resulting immune complex. Peroxidase activity was visualized using an aminoethyl carbazole substrate kit (Zymed Laboratories, Inc., San Francisco, CA).

Animals and in vivo tumorigenicity assay

All the animals and their care were treated and conducted according to the national and international laws and policies (Guide for the Care and Use of Laboratory Animals, published by National Institutes of Health, 8th ed., Guide2011; Checklist modified by Chinese-Taipei Society of Laboratory Animal Sciences from Animal Association for Assessment and Accreditation of Laboratory Animal care). The experimental protocol was approved by the National Cheng Kung University Institutional Review Board (Number 106067). The study was conducted according to the ARRIVE (Animal Research Reporting In Vivo Experiments) requirements (detailed in Supplementary Table 1).

To explore the tumorigenic effect of *EP1* expression in RCC-RF phenotype, we conducted the xenograft tumor mode in mice. Briefly, eight-week-old female nonobese diabetic/severe combined immunodeficiency (NOD/SCID) mice were purchased from the NCKU Laboratory Animal Center and maintained in a pathogen-free facility under isothermal conditions with regular photoperiods. In the morning of the day (around 10AM), ACHN *INI1* KD cells or ACHN *INI1* & *EP1* double KD cells were harvested from cultured dishes and re-suspended in serum-free RPMI1640 media. A total of 16 mice were randomly separately into two groups ($n = 8$ each group) and were subcutaneously injected into the loose skin on the flank either with ACHN *INI1* KD cells or ACHN

INI1 & EP1 double KD cells (1×10^6 cells) in 100 μl serum-free medium. This injection was carried out just outside the cage in a standard procedure (*i.e.*, in the hand-maintaining procedure using holding between the scruff and tail base of the mice) without anesthesia and analgesia. No other experiment procedures or treatment was done except the observation and recording the tumor formation and growth every other day for at least 80 days according to the ARRIVE Guidelines for Reporting Animal Research. Tumor volumes were calculated using the formula: length $\times$ (width)^2 $\times$ 0.45. Finally, mice were euthanized at the end of the experiment using intraperitoneal injection of Pentobarbital (60–100 mg/kg).

Data analysis and statistics

All of experiments were carried out in triplicate and numerical data were presented as mean ± SEM. Student's t-test was used to compare the difference between each group. Only variables of $p < 0.05$ were considered significant.

Results

The potential significance of INI1 in the pathogenesis of RCC-RF

To investigate the significance of *INI1* in the pathogenesis of RCC-RF, we first examined the rhabdoid differentiation area of RCCs using strict criteria as previously described [9–10] and paired non-neoplastic kidney. Frozen tissue samples ($n = 5$) from our cancer database were dissected for real-time PCR analysis (Fig. 1a) and western blotting (Fig. 1b). Downregulation of *INI1* at both transcriptional and translational levels was demonstrated in the tissue showing rhabdoid differentiation compared with non-neoplastic kidney control. IHC for INI1 expression was performed on 8 RCC-RF samples, including those of frozen tissue collected for real-time PCR. An apparent loss of INI1 protein expression was clearly demonstrated in the nuclei of the rhabdoid cells (Fig. 1c-III and IV), as opposed to ccRCC component (Fig. 1c-I and II). Four of the patients died of cancer, and one was alive with progressive disease despite targeted therapy (Table 1).

To explore the mechanisms underlying *INI1*-mediated tumorigenesis of RCC-RF, stable ACHN *INI1* KD clone was created (Fig. 2). Stable ACHN *INI1* KD cells showed rhabdoid differentiation with large, eccentric nuclei and prominent nucleoli (arrows in Fig. 2a). Expression of *INI1* was significantly suppressed at mRNA and protein levels in *INI1* KD cells (Fig. 2b& 2c). Expression of E-cadherin (epithelial marker) was downregulated in sable ACHN *INI1* KD cell line compared with parental cells, while both Snail (a key transcriptional repressor of E-cadherin expression in epithelial-mesenchymal transition) and EGFR were upregulated after knocking down of *INI1* (Fig. 2d).

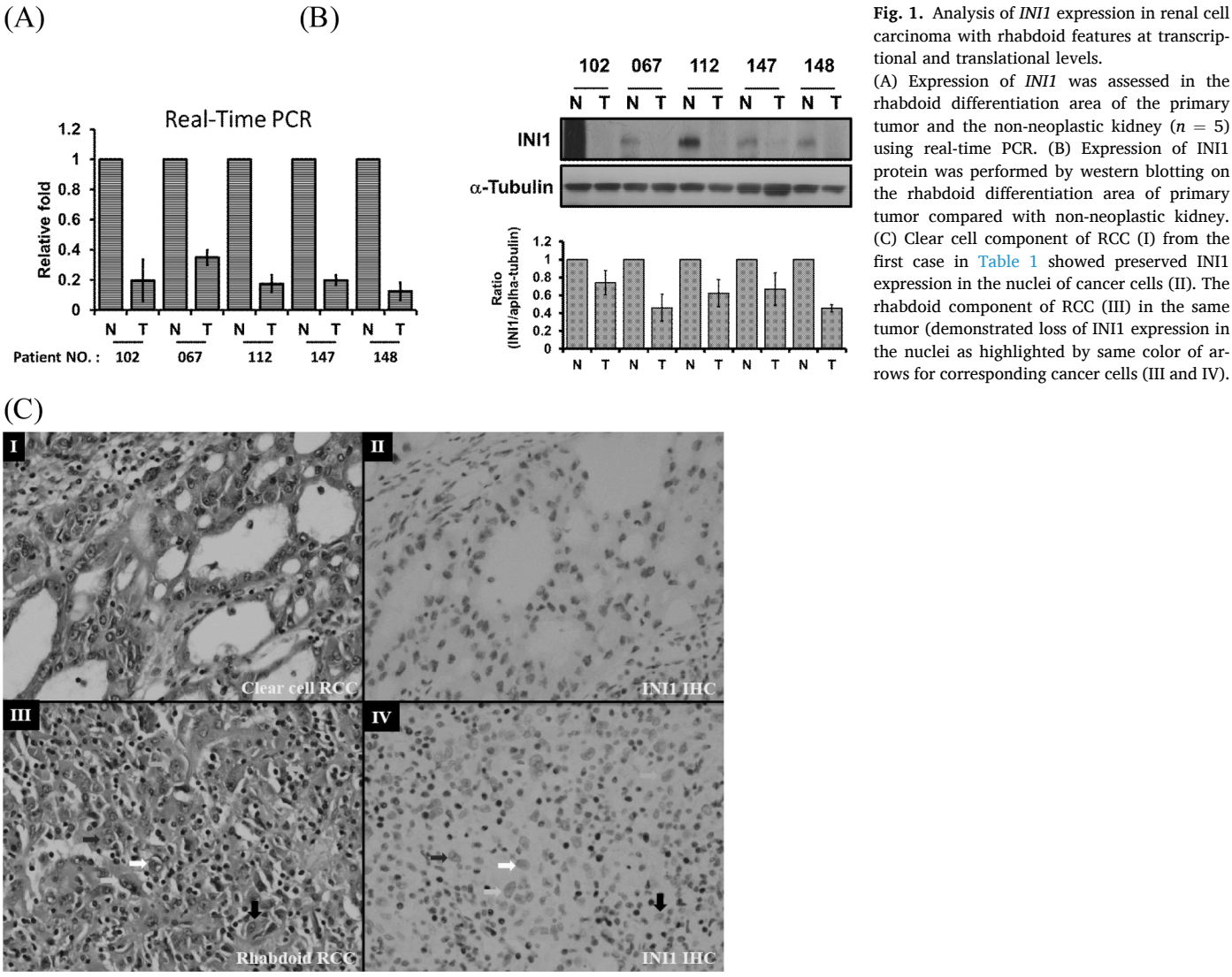

Fig. 1. Analysis of *INI1* expression in renal cell carcinoma with rhabdoid features at transcriptional and translational levels.
(A) Expression of *INI1* was assessed in the rhabdoid differentiation area of the primary tumor and the non-neoplastic kidney ($n = 5$) using real-time PCR. (B) Expression of INI1 protein was performed by western blotting on the rhabdoid differentiation area of primary tumor compared with non-neoplastic kidney. (C) Clear cell component of RCC (I) from the first case in Table 1 showed preserved INI1 expression in the nuclei of cancer cells (II). The rhabdoid component of RCC (III) in the same tumor (demonstrated loss of INI1 expression in the nuclei as highlighted by same color of arrows for corresponding cancer cells (III and IV).

Table 1
Clinical summary of clear cell RCC with rhabdoid features.

Age	Sex	Stage /Grade	TTM	Metastasis	INI1 expression	Sequential Rx	TT Length	Outcome (OS after TT)
60	M	pT2N0M0/3	6m	Lung, scalp, Lymph node	Loss	IL-2, Xeloda, sorafenib (15 m), sunitinib (25 m), everolimus (3 m),	43 m	Dead with PD (4y5m)
60	M	pT2N0M0/3	12m	Lung	Loss	Sunitinib (6 m), everolimus (18 m)	18m	Alive with PD (36 m)
48	M	pT3N2M0/4	2m	Lung	Loss	Sunitinib (6 m), Temsirolimus (0.5 m)	6.5 m	Dead with PD (10 m)
72	F	pT3aN0M0/4	5m	Brain, Lung	Loss	Temsirolimus (3 m)	3m	Dead with PD (3 m)
59	F	pT3aN0M+/3	0	Lung, adrenal gland	Loss	Sunitinib (6 m)Everolimus (6 m)	12m	Dead with PD (12 m)
79	F	pT2N0M0 /3	2m	SC, lung	Loss	Sunitinib (12 m), Everolimus (6 m)	18m	Alive (18 m)
65	M	pT2N2M+ /4	0	Lung, lymph node	Loss	Temsirolimus (3 m)	3m	Alive (3 m)
70	M	T3aN0M1 /4	0	Lung	Loss	Sunitinib (3 m)	3m	Alive (3 m)

TTM, time of diagnosis to metastasis; SC, subcutaneous, PD, progressive disease.
TT: Targeted therapy.

Effect of INI1 on cell proliferation, migration and invasion in vitro

In terms of biological effects, MTT assays showed that growth rate of stable ACHN *INI1* KD cells was significantly higher compared with vector control cells ($p < 0.05$) (Fig. 3a). Cell migration was also significantly increased (2.37 times) as was transwell invasion (2.5 times) *in vitro* (Fig. 3b-c). However, stable 786-O *INI1* KD cells showed lower cell growth and migration rate *in vitro* compared with vector control cells ($p < 0.05$, respectively) (Supplementary Fig. 1).

The importance of INI1 in the modulation of signaling pathway in RCC-RF

Because EGFR expression was increased (1.96 folds) in ACHN *INI1* KD cells compared with vector control (VC) (Fig. 2d), the potential functional relevance in RCC was investigated. EGF is known to be produced by renal tubular cells and secreted into human urine [26]. We showed that EGF treatment (10 ng/mL) stimulates the expression of phospho-EGFR in stable ACHN *INI1* KD cells in a dose-dependent manner (Fig. 3d), with comparable trend observed for phosphor-AKT (ser473) too. More importantly, elevated phospho-EGFR expression (3.4 folds) was demonstrated as early as 0.5 min after EGF treatment to ACHN *INI1* KD cells. In addition, both phospho-ERK and phosphor-AKT (ser473) were upregulated in stable 786-O *INI1* KD cells (Supplementary Fig. 2), supporting that EGFR pathway is activated in *INI1*-related RCC *in vivo*.

To evaluate the drug sensitivity *in vitro*, doses of conventional RCC therapeutics were tested, including capecitabine, Sorafenib, Sunitinib, Everolimus, Avastin, Erlotinib and Gefitinib. Cell viability assay showed that ACHN *INI1* KD cells were sensitized to Erlotinib and Everolimus treatment *in vitro* compared with vector control ($P < 0.05$) (Fig. 4). The Gefitinib treatment showed trivial effect only. In contrast, knocking down of *INI1* resulted in resistance of ACHN cells to Sorafenib treatment ($P < 0.05$) (Fig. 4). There was no difference of sensitivity to capecitabine, Sunitinib or Avastin (data not shown). The results suggest that downregulating *INI1* activates the EGFR and mTOR signaling pathways in pRCC.

To verify the above observations, stable 786-O *INI1* KD cells were tested with Erlotinib, Everolimus or Gefitinib. As with ACHN *INI1* KD cells, knocking down of *INI1* sensitized 786-O cells to Erlotinib treatment *in vitro* compared with vector control ($P < 0.05$) (Supplementary Fig. 3). To our surprise, stable 786-O *INI1* KD cells became more resistant to Gefitinib and Everolimus treatment *in vitro* ($P < 0.05$, respectively) (Supplementary Fig. 3).

Given inconsistent chemosensitivity *in vitro* was observed for stable *INI1* KD cells, a cDNA microarray analysis was performed on ACHN parental cell line and stable *INI1* KD cells to identify additional potential therapeutic targets. A total of 1024 genes were suggested to be upregulated in association with *INI1* KD (supplementary Table 2) [27]. Some of these genes, such as EGFR, are known to be involved in the pathogenesis of RCC [28]. The accuracy of profiling was preliminarily supported by western blotting for EGFR (Fig. 2D). In addition, VEGF-A165 was found to be upregulated when *INI1* was knocked down in both ACHN and 786-O cells (data not shown). The significance of regulation of VEGF-A165 and VEGF-C expression by *INI1 in vivo* was confirmed using IHC on primary tumor and metastases of the first case in Table 1 (supplementary Fig. 4).

Signaling crosstalk between PGE2/EP1 and EGFR in INI1 KD stable cells

Among candidate genes, the *EP* family was further chosen for investigation because of its involvement in VEGF-mediated carcinogenesis and a crosstalk with EGFR [29]. RT-PCR screening showed that both *EP1* and *EP4* are upregulated (1.20 times and 1.57 times, respectively) in stable ACHN *INI1* KD cells compared with vector control cells (Fig. 5a). Western blotting confirmed slightly elevated expression of EP1 (1.26 folds) and EP4 (1.31 folds) proteins in stable ACHN *INI1* KD cells than vector control (Fig. 5b).

In our microarray experiment, a higher expression of PGE2 synthase-COX1 (1.32 times) was demonstrated when *INI1* was knocked down in ACHN cells (Supplementary Fig. 5a). Expression/secretion of PGE2 was higher (1.36 times) in stable ACHN *INI1* KD cells compared with vector control (Supplementary Fig. 5c). In contrast, *COX2* was not expressed in ACHN cells (Supplementary Fig. 5b). To elucidate the crosstalk of signaling pathway between PGE2/EP1 and EGFR, expression of phosphorylation of AKT and ERK was examined after PGE2 treatment.

Treatment of PGE2 (10 μM) exhibited a dose-dependent stimulation of AKT phosphorylation in ACHN *INI1* KD cells *in vitro* compared with ACHN VC cells (Fig. 5c). With a background of persistent higher EGFR expression in ACHN *INI1* KD cells, PGE2 treatment tends to stimulate phospho-AKT expression with time compared with steadily suppressed expression in ACHN VC cells (Fig. 5d). Likewise, PGE2 treatment induced a sustained ERK1/2 phosphorylation compared with a time-dependent suppression in the ACHN VC cells. The results highly suggest the existence of a signaling crosstalk between PGE2/EP1 and EGFR in *INI1*-related pRCC.

The involvement of INI1/PGE2 related signaling pathway in RCC-RF

To examine the potential crosstalk between PGE2 signaling and related pathway, *INI1* and *EP1* stable pool of double KD cells were prepared. Expression of *INI1* and *EP1* were verified at both mRNA and protein levels (Supplementary Fig. 6). Because expression of INI1 was comparable in both ACHN *INI1* KD and ACHN *INI1/EP1* double KD cells (Supplementary Fig. 6b and 6c), ACHN *INI1/EP1* double KD cells were chosen as an experimental group compared with ACHN *INI1* KD (control group) for examination. Both growth rate (Fig. 6a) and migration

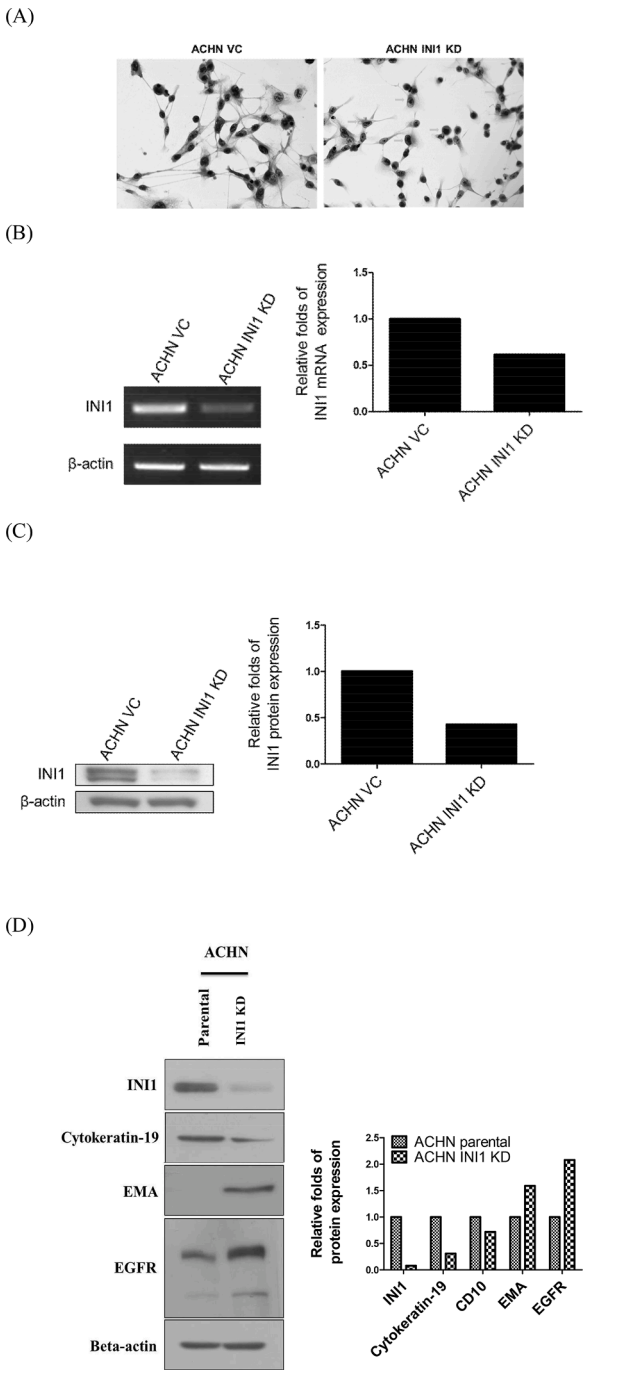

Fig. 2. Establishment of stable ACHN *INI1* KD cell line.
(A) The stable ACHN *INI1* KD cells showed rhabdoid differentiation with large, eccentric nuclei and prominent nucleoli. Expression of *INI1* was apparently downregulated at mRNA (B) and protein (C) levels in stable *INI1* KD cells compared with parental cells. (D) Biomarker expression screening showed that both CK-19 and CD10 are downregulated, while EMA is up-regulated in *INI1* stable KD cells. Interestingly, EGFR is apparently upregulated in *INI1* stable KD cells. Quantitation of each biomarker expression was demonstrated in the right panel.

(Supplementary Fig. 7) *in vitro* were significantly inhibited in stable *INI1/EP1* double KD cells compared with ACHN *INI1* KD cells ($p < 0.001$). The *in vivo* turmorigenicity assay showed that xenograft growth of ACHN *INI1* KD cells in NOD/SCID mice were significantly inhibited when *EP1* was also knocked down ($p < 0.001$) (Fig. 6b). A significantly higher proliferation rate *in vitro* was demonstrated for 786-O *INI1/EP1* double KD cells compared with vector control ($P < 0.05$) (Supplementary Fig. 8). Again, the result is contradictory to that of ACHN *INI1/EP1* double KD cells. We found that expression of phosphor-AKT (ser473) is not suppressed in stable 786-O *INI1/EP1* double KD cells, while both phospho-ERK and total ERK were down-regulated compared with vector control (Supplementary Fig. 9).

Discussion

Rhabdoid cells can be found in different subtypes of adult RCC [9–14], with most frequently reported in ccRCC [9]. RCC-RF are usually associated with high-grade histology, advanced clinical staging, sarcomatoid dedifferentiation, and are considered the endpoint of clonal evolution [9–16, 30]. We provide direct evidence that expression of *INI1* is down-regulated in RCC-RF at both transcriptional and translational levels. This is consistent with two recent studies [23,24], but not with earlier report [13] that showing retained nuclear INI1 staining. Although combined loss of BAP1 and PBRM1 was reported to associate with rhabdoid histology of RCC [21], BAP1 expression was inhibited in stable ACHN *INI1* KD cells; however, PBRM1 protein was not expressed in ACHN cells in our model (data not shown). Our findings suggest that down-regulation of *INI1* may play a role in the pathogenesis of RCC-RF. In addition, the efficacy of *INI1* in modulating VEGFs provides further support for its significance for RCC-RF. Thus, this investigation identified particular molecular mechanisms underlying *INI1* inactivation in the pathogenesis of RCC-RF, in addition to *BAP1* and *PBRM1* [21].

The current paradigm of RCC therapy is targeted therapies, *e.g.*, anti-VEGF-A antibody (Bevacizumab), VEGFR2 TKIs (Sunitinib and Sorafenib), or mTOR inhibitors (Temsirolimus and Everolimus). Targeted drugs are especially important when chemotherapy is ineffective for RCCs and are often given as first-line treatment in metastatic disease [31]. However, there is no consensus on which drug is the best. We found that EGF within normal urinary concentration range upregulated EGFR and its downstream PI3K/AKT and MAPK pathways in stable ACHN *INI1* KD cells, with comparable results in 786-O *INI1* KD cells. The increased sensitivity of stable *INI1* KD cells to Erlotinib *in vitro* in both pRCC and ccRCC model cell lines concurs with Darr et al. [32], which demonstrated *INI1*-dependent phosphoryation of EGFR and its downstream signaling with increased sensitivity of *Smarcb1* deficient cells to EGFR signaling inhibitor. The result also concurs with recent report showing that erlotinib in combination with bevacizumab is clinically active against INI1-negative renal medullary carcinoma [33]. Together, our findings support that Erlotinib could be considered in the management of patients with RCC-RF.

However, conflicting *in vitro* response of stable *INI1* KD cells to Everolimus and Gefitinib between pRCC and ccRCC model cell lines is noteworthy. Likewise, activation of AKT and ERK pathways in *INI1*-related pRCC by PGE2 treatment *in vitro* supports for a signaling cross-talk between EP and EGFR [34]. The growth of ACHN *INI1/EP1* double KD cells *in vitro* and *in vivo* seems to support the implication of PGE2/EP1 pathway inhibitor in the treatment of RCC-RF. To our surprise, expression of VEGF-A was inhibited together with upregulated VEGF-C in *INI1* KD and *EP1* KD cells (Supplementary Fig. 4); however, divergent effects were observed when *EP1* was knocked down on 786-O *INI1* KD cells *in vitro* (Supplementary Fig. 8). Thus, whether inhibiting *EP1* pathway could activate superfluous signaling requires further investigation. Currently, we have no experimental data to justify the inconsistency. A differential network of oncogenic signaling pathways between *c-MET* mutation and *VHL*-defective RCCs maybe the most plausible explanation. On the other hand, this investigation highlights the impact of subtype-specific molecular abnormalities on the selection of molecularly targeted approaches for patients with RCC.

Conclusion

In summary, loss of INI1 expression was demonstrated in adult RCC-

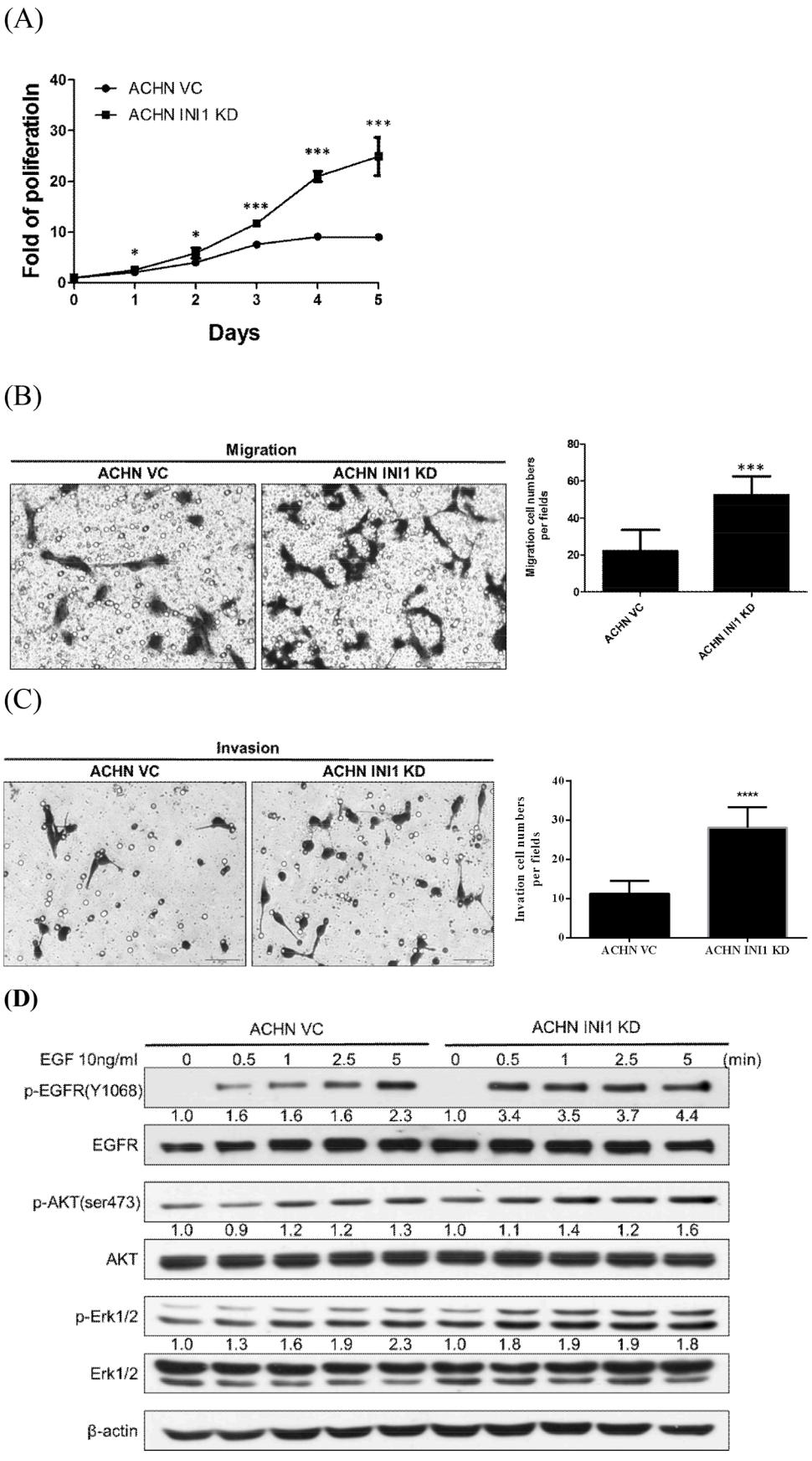

Fig. 3. Effect of *INI1* on cell proliferation, migration, and invasion *in vitro*.
(A) ACHN *INI1* KD cells showed a significantly higher proliferation rate *in vitro* compared with vector control cells. Data are representative of 3 independent experiments and expressed as mean ± SD ($P < 0.05$; *t*-test). (B) An increased cell migration was demonstrated for *INI1* KD cells than vector control cells. Quantitation data are representative of 3 independent experiments and expressed as mean ± SD ($P < 0.05$: *t*-test). (C) Cell invasion assessed by transwell assay was also higher in *INI1* KD cells than vector control. Quantitation data are representative of 3 independent experiments and expressed as mean ± SD ($P < 0.001$; *t*-test). (D) Cells were starved for 24 h and then treated with EGF (10 ng/mL) for different periods. Expression of phosphorylation status of EGFR, AKT, and ERK1/2 was examined by immunoblotting. The phospho-EGFR and phosphor-AKT (ser473) were upregulated in stable ACHN *INI1* KD cells. The ratio of p-EGFR, p-AKT, and p-ERK1/2 was normalized using total protein as a reference.

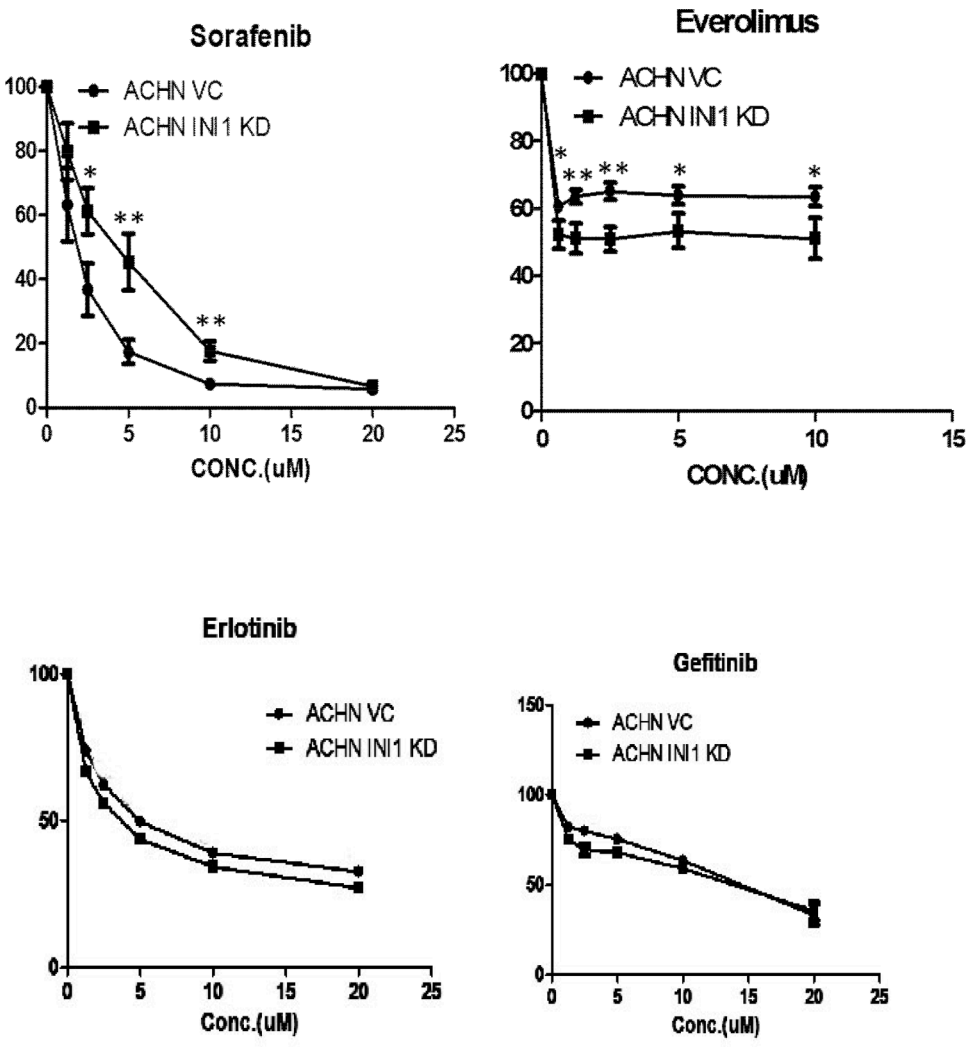

Fig. 4. Response of ACHN *INI1* KD cells to target therapy *in vitro*.
The *INI1* KD cells were tested for sensitivity to target therapy *in vitro*. Cells (1×10^3/ well) were seeded in 96-well plates. After incubation with anticancer drug for 72 h, MTT reagent was added for 4 h to a final concentration of 0.5 mg/mL. The absorbance of formazan was measured at 570 nm. Dimethylsulfoxide was used as a control. Our data showed that ACHN *INI1* KD cells were sensitized to Everolimus or Erlotinib treatment *in vitro*. Data are representative of 3 independent experiments and expressed as mean ± SD ($P < 0.05$: *t*-test).

RF and down-regulation of *INI1* may contribute to the pathogenesis of RCC-RF. Erlotinib is recommended in the treatment of *INI1*-related RCCs. More research is needed to clarify the efficacy of second and third generations of TKIs in the treatment of RCC-RFs.

Funding

This manuscript was supported by research grant NSC98-2320-B-006-022-MY3 from the Ministry of Science and Technology, TAIWAN; NCKUH-10605017 and NCKUH- T10809020 from the National Cheng Kung University Hospital, Tainan, TAIWAN.

Availability of data and materials

All authors include an "Availability of Data and Materials" section in our manuscript detailing where the data supporting their findings can be found.

Author contributions

YW Wang, HL Song: Designed and performed experiments, analyzed data and co-wrote the paper.

CA Chu, YL Tuan, KH Tsai, CY Chiang, HF Song, HY Chang: Performed experiments.

CA Chu, HY Chang: Performed bioinformatic analyses.

NH Chow, YS Tsai: Designed experiments and co-wrote the paper.

All authors have read and approved the manuscript.

Ethics approval and consent to participate

The experimental protocol adhered to the regulations of the Animal Protection Act of Taiwan and was approved by the NCKU Laboratory Animal Care and User Committee (106067). Attached the Supplementary Table 1 _ ARRIVE 20200417

Consent for publication

Not applicable.

Publisher's Note

Springer Nature remains neutral with regard to jurisdictional claims in published maps and institutional affiliations.

Authors' information (optional)

Yi-Wen Wang, Departments of Pathology, College of Medicine, National Cheng Kung University, TAIWAN

Hsiang-Lin Song, Department of Pathology, National Cheng Kung University Hospital, TAIWAN

Cheng-Yao Chiang, Departments of [1]Pathology, College of Medicine, National Cheng Kung University, TAIWAN

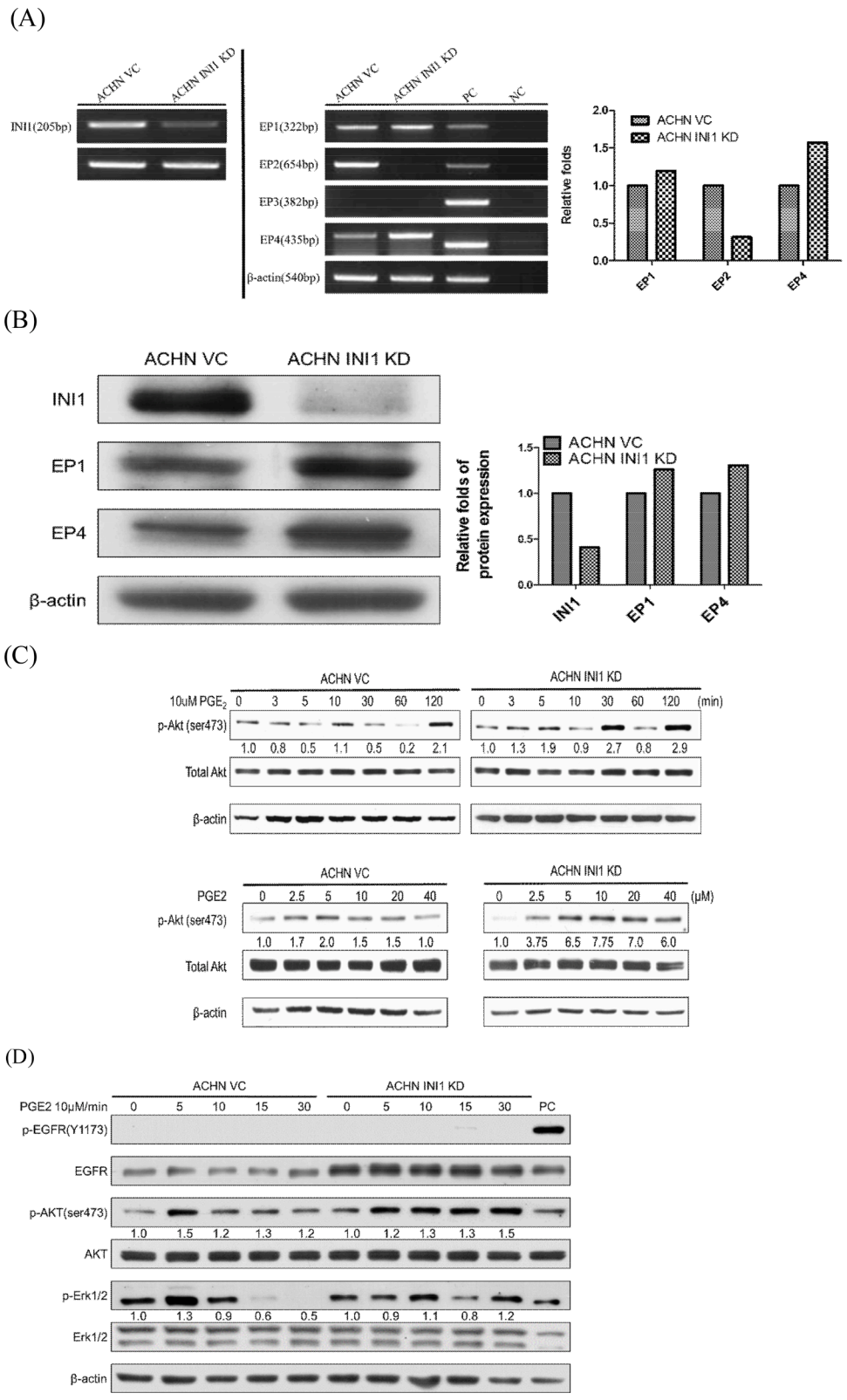

Fig. 5. Expression of prostaglandin E (PGE)-type receptor family and COX-2/ PGE2 pathway in *INI1* KD cells.
(A) Expression of endogenous PGE-type receptor family (*EP* family) was assessed using RT-PCR. The result of quantitation data was shown on the right panel. The sh-SY5Y cell line cDNA was used as a positive control. (B) Expression of EP1 & EP4 protein in *INI1* KD cells was assessed using western blot and quantitation data was shown on the right panel. Both *EP1* and *EP4* were upregulated in stable ACHN *INI1* KD cells analyzed by RT-PCR and western blotting. (C) A time- and dose-dependent activation of AKT phosphorylation was demonstrated in PGE2-treated cells. (D) The phosphorylation status of EGFR, AKT, and ERK1/2 were examined using immunoblotting. PGE2 treatment exhibited a time- and dose-dependent stimulation of AKT phosphorylation, and ERK1/2 phosphorylation was time-dependently upregulated too. The ratio of phospho-AKT and phospho-ERK1/2 was normalized using total protein as a reference.

Hong-Fang Song, Institute of Molecular Medicine, College of Medicine, National Cheng Kung University, TAIWAN

Hong-Yi Chang, Department of Biotechnology and Food Technology, College of Engineering, Southern Taiwan University of Science and Technology, TAIWAN

Chien-An Chu, Departments of Pathology, College of Medicine, National Cheng Kung University, TAIWAN

Yih-Lin Tuan, Institute of Molecular Medicine, College of Medicine, National Cheng Kung University, TAIWAN

Kun-Hao Tsai, Institute of Molecular Medicine, College of Medicine, National Cheng Kung University, TAIWAN

Nan-Haw Chow, Departments of Pathology and Institute of

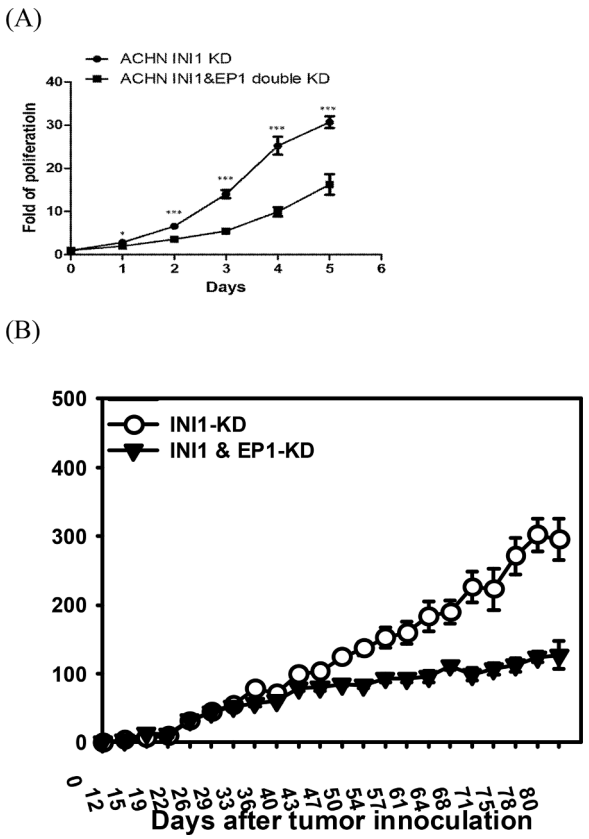

Fig. 6. Effect of *INI1* KD cells on *in vitro* and *in vivo*.
(A) The *INI1* KD & *EP1* double KD cells had a significantly lower proliferation ($P < 0.05$: *t*-test) than that of *INI1* KD cells ($p < 0.001$). Data are representative of three independent experiments and expressed as mean ± SD. (B) Six-eight-week-old female NOD/SCID mice were subcutaneously injected with 1×10^6 *INI1* KD cells or *INI1* KD & *EP1* double KD cells (each group: $n = 8$). The *in vivo* tumorigenicity assay showed that xenograft growth of *INI1* & *EP1* double KD cells was significantly ($P < 0.001$) inhibited compared with ACHN *INI1* KD cells.

Molecular Medicine, College of Medicine, National Cheng Kung University, TAIWAN

Yuh-Shyan Tsai Departments of Urology, College of Medicine, National Cheng Kung University, TAIWAN

Declaration of Competing Interest

The authors declare that they have no competing financial interests.

Acknowledgments

Not Applicable.

Supplementary materials

Supplementary material associated with this article can be found, in the online version, at doi:10.1016/j.tranon.2021.101175.

References

[1] Cancer Facts & Figures, American Cancer Society, 2020. Accessed: Jan 7, 2021.
[2] B. Escudier, Combination therapy as first-line treatment in metastatic renal-cell carcinoma, N. Engl. J. Med. 380 (2019) 1176–1178.
[3] A. Brodziak, P. Sobczuk, E. Bartnik, et al., Drug resistance in papillary RCC: from putative mechanisms to clinical practicalities, Nat. Rev. Urol. 16 (2019) 655–673.
[4] S. Ogino, T.Y. Ro, R.W Redline, Malignant rhabdoid tumor: a phenotype? An entity?–A controversy revisited, Adv. Anat. Pathol. 7 (2000) 181–190.
[5] P.B. Becker, W. Horz, ATP-dependent nucleosome remodeling, Annu. Rev. Biochem. 71 (2002) 247–273.
[6] L. Ho, G.R. Crabtree, Chromatin remodelling during development, Nature 463 (2010) 474–484.
[7] L.R. Donner, L.M. Wainwright, F. Zhang, et al., Mutation of the INI1 gene in composite rhabdoid tumor of the endometrium, Hum. Pathol. 38 (2007) 935–939.
[8] S. Medjkane, E. Novikov, I. Versteege, et al., The tumor suppressor hSNF5/INI1 modulates cell growth and actin cytoskeleton organization, Cancer Res. 64 (2004) 3406–3413.
[9] N. Gökden, O. Nappi, P.E. Swanson, et al., Renal cell carcinoma with rhabdoid features, Am. J. Surg. Pathol. 24 (2000) 1329–1338.
[10] B. Shannon, Z. Stan Wisniewski, J. Bentel, et al., Adult rhabdoid renal cell carcinoma, Arch. Pathol. Lab. Med. 126 (2002) 1506–1510.
[11] K. Kuroiwa, Y. Kinoshita, H. Shiratsuchi, et al., Renal cell carcinoma with rhabdoid features: an aggressive neoplasm, Histopathology 41 (2002) 538–548.
[12] X. Leroy, L. Zini, D. Buob, et al., Renal cell carcinoma with rhabdoid features: an aggressive neoplasm with overexpression of p53, Arch. Pathol. Lab. Med. 131 (2007) 102–106.
[13] J.X. Cheng, M. Tretiakova, C. Gong, et al., Renal medullary carcinoma: rhabdoid features and the absence of INI1 expression as markers of aggressive behavior, Mod. Pathol. 21 (2008) 647–652.
[14] P.A. Humphrey, Renal cell carcinoma with rhabdoid features, J. Urol. 186 (2011) 675–676.
[15] D. Brett, N.E. John, E. Lars, et al., Grading of renal cell carcinoma, Histopathology 74 (2019) 4–17.
[16] A. Kapoor, R. Tutino, A. Kanaroglou, et al., Treatment of adult rhabdoid renal cell carcinoma with sorafenib, Can Urol Assoc J 2 (2008) 631–634.
[17] G. Kats-Ugurlu, C. Maass, C. van Herpen, et al., Better effect of sorafenib on the rhabdoid component of a clear cell renal cell carcinoma owing to its higher level of vascular endothelial growth factor-A production, Histopathology 59 (2011) 562–564.
[18] F. De Vincenzo, P.A. Zucali, G.L. Ceresoli, et al., Response to sunitinib in an adult patient with rhabdoid renal cell carcinoma, J. Clin. Oncol. 29 (2011) e529–e531.
[19] R. Alessandro, M. Veronica, S. Matteo, et al., Impact of clinicopathological features on survival in patients treated with first-line immune checkpoint inhibitors plus tyrosine kinase inhibitors for renal cell carcinoma: a meta-analysis of randomized clinical trials, Eur. Urol. Focus 21 (2021) S2405–S4569.
[20] Q. Rao, Q.Y. Xia, Q. Shen, et al., Coexistent loss of INI1 and BRG1 expression in a rhabdoid renal cell carcinoma (RCC): implications for a possible role of SWI/SNF complex in the pathogenesis of RCC, Int. J. Clin. Exp. Pathol. 7 (2014) 1782. -1287.
[21] S. Pena-Llopis, S. Vega-Rubin-de-Celis, A. Liao, et al., BAP1 loss defines a new class of renal cell carcinoma, Nat. Genet. 44 (2012) 751–759.
[22] M. Veronica, F. Tania, G. Elisa, et al., Broad spectrum mutational analysis of chromophobe renal cell carcinoma using next-generation sequencing, Pathol. Res. Pract. 219 (2021), 153350.
[23] E. Sigauke, D. Rakheja, D.L. Maddox, et al., Absence of expression of SMARCB1/INI1 in malignant rhabdoid tumors of the central nervous system, kidneys and soft tissue: an immunohistochemical study with implications for diagnosis, Mod. Pathol. 19 (2006) 717–725.
[24] A. Agaimy, L. Cheng, L. Egevad, et al., Rhabdoid and undifferentiated phenotype in renal cell carcinoma: analysis of 32 cases indicating a distinctive common pathway of dedifferentiation frequently associated with SWI/SNF complex deficiency, Am. J. Surg. Pathol. 41 (2017) 253–262.
[25] M.M. Wolf, W. Kimryn Rathmell, K.E Beckermann, Modeling clear cell renal cell carcinoma and therapeutic implications, Oncogene 39 (2020) 3413–3426.
[26] N.H. Chow, T.S. Tzai, P.E. Cheng, et al., An assessment of immunoreactive epidermal growth factor in urine of patients with urological diseases, Urol. Res. 22 (1994) 221–225.
[27] N.H .SH. Chow, Y.S. Tsai, H.Y Chang, Development of therapeutics for renal cell carcinoma with rhabdoid features. New Horizons in Cancer Research: delivering Cures Through Cancer Science, Program Book, 2016, p. A0104.
[28] M.J. Stassar, G. Devitt, M. Brosius, et al., Identification of human renal cell carcinoma associated genes by suppression subtractive hybridization, Br. J. Cancer 85 (2001) 1372–1382.
[29] Y.B. Ding, R.H. Shi, J.D. Tong, et al., PGE2 up-regulates vascular endothelial growth factor expression in MKN28 gastric cancer cells via epidermal growth factor receptor signaling system, Exp. Oncol. 27 (2005) 108–113.
[30] C. Ciccarese, F. Massari, M. Santoni, et al., New molecular targets in non clear renal cell carcinoma: an overview of ongoing clinical trials, Cancer Treat. Rev. 41 (2015) 614–622.
[31] A. Daste, T. Grellety, M. Gross-Goupil, et al., Protein kinase inhibitors in renal cell carcinoma, Expert Opin. Pharmacother. 15 (2014) 337–351.
[32] O.F. Dajani, K. Meisdalen, T.K. Guren, et al., Prostaglandin E2 upregulates EGF-stimulated signaling in mitogenic pathways involving Akt and ERK in hepatocytes, J. Cell. Physiol. 214 (2008) 371–380.
[33] J.W. Andrew, S.S. Devaki, R. Priya, et al., Efficacy and Safety of Bevacizumab Plus Erlotinib in Patients with Renal Medullary, Carcinoma 13 (2021) 2170–2179.
[34] O.F. Dajani, K. Meisdalen, T.K. Guren, et al., Prostaglandin E2 upregulates EGF-stimulated signaling in mitogenic pathways involving Akt and ERK in hepatocytes, J. Cell. Physiol. 214 (2008) 371–380.